Droplet Evaporation Characteristics of Hydrotreated Vegetable Oil (HVO) Under High Temperature and Pressure Conditions

Leang So Khuong[a], Nozomu Hashimoto[a1], Yusuke Konno[a], Yusuke Suganuma[b], Hiroshi Nomura[b], and Osamu Fujita[a]

[a]Division of Mechanical and Space Engineering, Faculty of Engineering, Hokkaido University, Sapporo 060-8628, Japan

[b]College of Industrial Technology, Nihon University, Narashino, Chiba 275-8575, Japan

Abstract

To investigate hydrotreated vegetable oil (HVO) droplet evaporation characteristics under sub/trans/supercritical conditions, surrogate HVO droplet evaporation experiments were conducted under high temperatures (573-873 K) and pressures (0.1-2.0 MPa), and thermodynamic and physical properties were analyzed. The result reveals that HVO surrogate fuels have a lower density, surface tension, and boiling point, allowing better evaporation characteristics than diesel. HVO surrogate fuels exhibit shorter droplet lifetimes and higher evaporation rates than diesel under all ambient conditions. Among HVO surrogate fuels, HVO:C_{15}-C_{18}/isododecane has the shortest droplet lifetimes because adding iso-dodecane reduces the initial heating period due to a lower boiling point. It was found that the evaporation characteristics are affected by not only the boiling point but also fuel compositions and thermodynamic properties such as thermal conductivity, latent heat of vaporization, and specific heat of gas. Critical points (T_c, P_c) are important indicators for selecting evaporation conditions. Increasing temperature decreases droplet lifetime and increases the evaporation rate due to high heat transfer from the ambient gas. However, the effect of pressure on droplet lifetime relies on ambient temperature (T_{amb}). As pressure increases, droplet lifetime increases

[1] Corresponding author. Division of Mechanical and Space Engineering, Faculty of Engineering, Hokkaido University, Sapporo 060-8628, Japan. Tel.: 011 706-6388; E-mail: nozomu.hashimoto@eng.hokudai.ac.jp

at $T_{amb} < T_c$ and decreases at $T_{amb} > T_c$. Increasing pressure at $T_{amb} \sim T_c$ has no significant effect on droplet lifetime.

Keywords: Hydrotreated vegetable oil; Droplet evaporation; Multicomponent fuel; Diesel engines; High temperatures and pressures, Critical point

1. Introduction

Due to the increasing global warming issues, researchers have been committed to using renewable fuels for reducing carbon-based emissions in transportation, energy, and industrial sectors. It was reported that CO_2 emissions from industry, transportation, and power plants account for more than 80% of global CO_2 emissions[1] while the use of fossil fuels with combustion engines remains dominant until 2035. In Europe, it is strongly recommended to use renewable fuels in ICE-powered vehicles as a measure to comply with future emission targets and the Energy Directive which requires to fulfill at least 32% of its total energy needs with renewable energy by 2030[2]. Recently, hydrotreated vegetable oil (HVO) has attracted attention as a transport fuel from the viewpoint of environmental impact.

HVO is produced from vegetable oils, waste cooking oil, lignocellulosic material, algae lipids, and residue fat fractions coming from food, fish processing, and slaughterhouse industries[3]. HVO can be blended with diesel and used with compression ignition (CI) engines without hardware modifications, thus allowing direct CO_2 emission reduction from existing and new vehicles[2]. HVO has a higher heating value (43.86 MJ/kg) compared to diesel (42.60 MJ/kg)[4]. This indicates that the mass-based fuel consumption of HVO combustion is lower than that of diesel combustion. Unlike diesel, HVO contains mostly normal- and iso-alkane mixture without the composition of cycloalkanes and aromatics, resulting in a high cetane number and low soot tendency which is more suitable for CI engines[5,6]. Moreover, due to the isomerization process, the main issue of HVO associated with its poor low-temperature properties including high pour point, high cloud point, and high cold filter plugging point

(CFPP) can be adjusted according to regional and seasonal weather[3,7], therefore making HVO more beneficial and attractive compared to biodiesel.

Figure 1 illustrates the distillation curves of EN590 diesel, fatty acid methyl esters (FAME), HVO, and HVO-diesel blend. This curve indicates how each fuel evaporates at various temperatures under atmospheric pressure. HVO has a flatter distillation range compared to EN590 diesel. Initially, HVO has a higher initial distillation temperature than diesel due to the lack of light-end components with lower boiling points which are necessary for engine start-up[8]. However, at the latter stage, HVO exhibits a lower distillation temperature than diesel. This indicates that HVO contains more heavy-end components with lower final boiling points, thus leading to faster evaporation, shorter droplet lifetime, complete combustion, and tailpipe emission reduction[6]. FAME has the worst distillation characteristics due to heavier components while adding 30% HVO into EN590 diesel enhances the distillation characteristics compared to pure diesel.

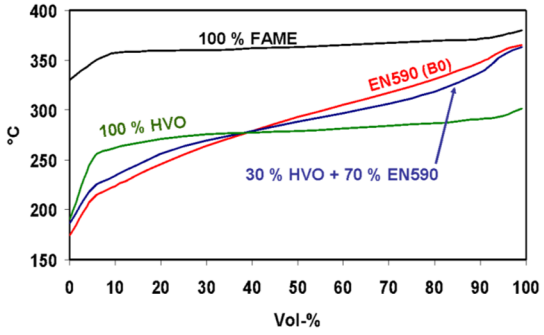

Fig. 1. Distillation curves of EN590 diesel, FAME, HVO, and HVO-diesel blend[8].

Spray characteristics, combustion, engine performance, and emissions of HVO have been investigated. For instance, Kim et al. investigated engine performance and emission characteristics of biodiesel (B100), HVO, and iso (isomeric)-HVO in light-duty diesel engines[5]. It was highlighted that iso-HVO yielded better engine power and fuel efficiency than B100 and HVO due to its higher cetane value, and calorific value. Iso-HVO and HVO emitted less HC and CO and a similar level of NO_x and PM compared to diesel, B100, and

biodiesel-diesel blends. The emission characteristics of five city buses fueled with EN590, HVO, FAME, and gas-to-liquid fuel (GTL) were investigated by Murtonen et al.[9]. The result showed that PM was reduced by 30-51% when running on paraffinic fuels (GTL and HVO). Recently, Han et al. investigated the ignition and combustion characteristics of hydrotreated pyrolysis (HPO), HVO, and diesel[10]. They found that the ignition delay followed the order of HVO < diesel < HPO. Blending HPO into HVO resulted in identical ignition and combustion behavior to diesel. It was suggested that HPO and HVO can be used to fuel modern marine engines to provide power to future mobility. Li et al investigated the combustion characteristics of HVO, ultra-low sulfur diesel (ULSD), and tallow methyl ester (TME) at different ambient temperatures using a constant-volume vessel [11]. Similarly, HVO had the shortest ignition delay, thus resulting in the longest combustion duration due to the highest cetane number while ULSD had the longest ignition delay. Under tested conditions, the combustion duration of HVO increased with increasing temperature while the combustion duration of HVO30, TME, and their blends initially decreased to the lowest value at 560℃ and then increased as temperature further increased. Hulkkonen et al. investigated the spray characteristics of HVO and diesel using a high-pressure injector[12]. The result revealed that HVO yielded a larger spray cone angle (SCA) compared to diesel, due to its lower viscosity and density. Bohl et al. also found that HVO exhibited a slightly larger SCA and a shorter spray penetration than diesel. [13].

Understanding multi-component droplet evaporation is crucial to optimizing the combustion of internal combustion engines, gas turbines, boilers, and liquid rocket engines. If fuel droplets are not evaporated in a timely manner, several issues such as incomplete combustion, knocking and high emissions may occur[14]. Faster evaporation of fuel droplets leads to a faster burn rate, which results in complete combustion, and low emissions[15]. Some researchers have experimentally investigated the evaporation characteristics of biodiesel and diesel[16,17] and biodiesel-ethanol blends [18] while both experimental and numerical studies

on droplet evaporation at high ambient temperature and pressure conditions have been conducted[19–21]. However, the study on HVO droplet evaporation has not been reported as far as the authors know while the droplet evaporation experiments under sub/supercritical conditions are inadequate. Therefore, in this study, HVO droplet evaporation is investigated under high temperature and pressure conditions. Thermodynamic and physical properties analysis and evaporation characteristics as well as the effects of temperatures and pressures on droplet evaporation are presented. This finding is significant for optimizing fuel injection strategies and the combustion efficiency of heavy-duty engines operated under various in-cylinder conditions.

2. Experimental methods

2.1 Fuel preparation

HVO surrogate mixtures having similar physical properties to diesel were formulated based on the components found in Gas Chromatography. Generally, HVO contains mostly four main n-alkanes such as n-pentadecane, n-hexadecane, n-heptadecane, and n-octadecane, which are commercially available hydrocarbons[5]. Iso-alkanes: isooctane and isododecane were added individually to resemble and match the physical properties of an algal HVO[7]. Three HVO surrogate mixtures were formulated based on the mass fraction determined in Ref [22], as listed in Table 1. For example, HVO:C_{15}-C_{18}/isododecane contains 9.30, 13.80, 26.50, 19.30, 31.10% of n-$C_{15}H_{32}$, n-$C_{16}H_{34}$, n-$C_{17}H_{36}$, n-$C_{18}H_{38}$, and iso-$C_{12}H_{26}$, respectively. Using Eq. (3.1), the averaged chemical formula of HVO:C_{15}-C_{18}/isododecane can be described as $C_{15.31}H_{32.61}$[23], which is close to the chemical formula estimated by Lapuerta et al.[7].

$$x, y = MW_{\mathrm{HVO}} \times (\%X, Y) \times (1/100) \times (1/a_{\mathrm{C,H}}) \tag{3.1}$$

where x and y are carbon (C) and hydrogen (H) atoms number, MW_{HVO}: molecular weight calculated based on mass fraction, $\%X$ and $\%Y$: atomic mass percentage, and $a_{\underline{C,H}}$: molar mass of carbon and hydrogen (g/mol).

Table 1. Components for HVO surrogate mixtures used in this study

	component (% mass fraction)					
Fuel name	n-$C_{15}H_{32}$	n-$C_{16}H_{34}$	n-$C_{17}H_{36}$	n-$C_{18}H_{38}$	iso-C_8H_{18}	iso-$C_{12}H_{26}$
HVO:C_{15}-C_{18}	13	20	39	28	0	0
HVO:C_{15}-C_{18}/isooctane	13.13	19.54	37.7	27.4	2.23	0
HVO:C_{15}-C_{18}/isododecane	9.3	13.8	26.5	19.3	0	31.1

iso-$C_{12}H_{26}$: 2,2,4,6,6-pentamethyl heptane (iso-dodecane)
iso-C_8H_{18}: 2,2,4-trimethylpentane (iso-octane)

Table 2 lists the properties of pure hydrocarbons such as n-$C_{12}H_{26}$, C_{15}-C_{18} alkanes, iso-C_8H_{18}, and iso-$C_{12}H_{26}$. Lighter components have a lower density, viscosity, boiling point, and surface tension than heavier components. For example, n-$C_{12}H_{26}$ has a lower boiling point than n-$C_{18}H_{38}$. This indicates that adding n-$C_{12}H_{26}$ lowers the boiling point of the HVO surrogate mixture, which enhances the evaporation characteristics. It is also observed that iso-$C_{12}H_{26}$ has a lower boiling point, flash point, melting point, and surface tension than n-$C_{12}H_{26}$. Therefore, the presence of iso-alkane in the HVO surrogate mixtures improves not only evaporation and combustion characteristics but also cold-flow characteristics. Properties such as boiling point, molecular weight, and specific gravity are used to calculate the averaged boiling point and critical properties of HVO surrogate fuels in section 2.2.

Table 2. Properties of each pure hydrocarbon

Properties	Unit	n-$C_{12}H_{26}$	n-$C_{15}H_{32}$	n-$C_{16}H_{34}$	n-$C_{17}H_{36}$	n-$C_{18}H_{38}$	iso-C_8H_{18}	iso-$C_{12}H_{26}$
Density @ 20°C	g/cm^3	0.749	0.768	0.773	0.778	0.782	0.692	0.7415
Viscosity@25 °C	mm^2/s	1.98	2.558	3.063	3.607	N/A	0.467	1.77 @ 20°C
boiling point	°C	216.3	270	286.9	302	316.3	99.2	177.8
flash point	°C	71	132.2	135	149	154-166	-12	45
melting point	°C	-9.55	9.9-15	18	22-24	28-30	-107	-67

Molecular weight	g/mol	170.34	212.42	226.47	240.47	254.50	114.23	170.34
Specific gravity	-	0.750	0.770	0.773	0.777	0.782	0.692	0.740
Surface tension @ 25°C	mN/m	24.69	26.68	27.09	27.52	N/A	18.32	21.6@22 °C

133

134 2.2 Critical properties calculation

135 The critical temperature (T_c) of a pure substance is the temperature above which the vapor
136 of the substance cannot be liquefied, no matter how much pressure is applied while the critical
137 pressure (P_c) is the minimum pressure required to liquefy a gas at its critical temperature.
138 Liquid and gas cannot coexist at any temperature if ambient pressure is higher than critical
139 pressure [24]. For combustion optimization, it is significant to understand the evaporation
140 characteristics of a single droplet at conditions below and above critical conditions. Critical
141 pressures and temperatures are not usually measured for hydrocarbon mixtures and must
142 therefore be estimated from correlation. The T_c and P_c of HVO surrogate mixtures were
143 calculated using a simple Riazi-Daubert correlation as expressed in Eq. (3.2) [25]. Yu et al.
144 used this correlation to determine the critical properties of some Jet fuels and obtained
145 satisfactory predictions of the critical temperatures of the petroleum-derived jet fuel[26]. Thus,
146 the following Riazi-Daubert correlation was also applied to estimate the T_c and P_c of HVO
147 surrogate fuels.

148 $$\theta = a[exp(b\theta_1 + c\theta_2 + d\theta_1\theta_2)]\ \theta_1^e\ \theta_2^f \quad (3.2)$$

149 In Eq. (3.2), θ represents the properties to be determined such as T_c, in [˚R], and P_c in [psia].
150 The determined properties were then converted to SI units. θ_1 and θ_2 refer to two parameters
151 corresponding to each property. Pairs of components: boiling point (T_b) and molecular weight
152 (MW) in g/mol, or MW and specific gravity (SG) are used to replace θ_1 and θ_2. *a, b, c, d, e,* and
153 *f* are correlation constants. Appendix A lists the constants used in Eq. (3.2). For mixtures
154 containing iso-alkane, only correlations with pair of parameters (T_b, SG) can be applied

because the boiling points of iso-alkane and n-alkane are different. The average MW, SG, and T_b of HVO surrogate mixtures were calculated based on the mass fraction of each component using Eq. (3.3). The detailed calculations are described in Appendix B.

$$A = \sum_{i=1}^{N} x_{wi} B_i \quad (3.3)$$

Where A refers to MW, SG, or T_b of mixtures, $x_{wi} = w_i/w_{tot}$ is the mass fraction of the species i in an HVO surrogate mixture, and B_i represents MW, SG, or T_b of the species i.

2.3 Thermodynamic and physical properties analysis

Table 3 lists the thermodynamic properties of pure hydrocarbons. Generally, a higher boiling point leads to a longer initial heating period and prolongs the droplet lifetime[27]. This indicates that the droplet lifetime is longer for heavier hydrocarbons. Critical points (T_c, P_c) are important indicators for selecting the evaporation conditions of a fuel. For example, iso-$C_{12}H_{26}$ has a lower boiling point (T_b = 450.80 K) and critical temperature (T_c = 652.25 K) with slightly higher critical pressure (P_c = 19.2 bar) compared to n-$C_{12}H_{26}$ (T_b = 489.47 K, T_c = 658.20 K, and P_c = 18.24 bar), which indicates that evaporation characteristics are enhanced, and broader efficient evaporation conditions can be obtained under actual combustion process. The coupling effect of T_c and P_c on evaporation characteristics is further discussed in section 3.3 while the thermal conductivity (λ) and specific heat (C_p) of each fuel are used to support the discussion of evaporation characteristics of HVO surrogate fuels in section 3.2.

Table 3. Thermodynamic properties of pure hydrocarbons

Properties	iso-C_8H_{18}	iso-$C_{12}H_{26}$	n-$C_{12}H_{26}$	n-$C_{15}H_{32}$	n-$C_{16}H_{34}$	n-$C_{17}H_{36}$	n-$C_{18}H_{38}$
T_b [K]	372.2	450.80*	489.47	543.83	560.01	575.30	589.86
Tc [K]	544.0	652.25	658.20	706.80	720.60	733.37	745.26
P_c [bar]	25.6	19.2	18.24	15.20	14.19	13.17	12.14
λ_L @ 30°C [W/m K]	0.09899	0.12462**	0.13567	0.13935	0.13975	0.14414	0.14968
C_{pL} @ 30°C [J/(g K)]	2.04392	2.10357**	2.22177	2.22445	2.22864	2.30719	2.29681

λ_L/C_{pL} [g/m s]	0.04843	0.05924	0.06107	0.06265	0.06271	0.06248	0.06517

*: Value calculated based on molecular structure using Ambrose and Townsend correlation[28]
**: Value calculated based on group contribution using Latini et al. correlation[29].
λ and C_p are calculated based on the correlation described in Chemical Properties Handbook[30].

Table 4 lists the properties of HVO fuels and diesel. Compared to diesel, HVO:C_{15}-C_{18} exhibits lower density and surface tension but much higher viscosity. However, after adding branching alkane (isooctane and isododecane), density, viscosity, and surface tension are lowered, allowing HVO:C_{15}-C_{18}/isododecane to exhibit similar physical properties to algal HVO. The critical temperature and pressure of HVO surrogate fuels were calculated using Eq. (3.2). It can be observed that the range of critical temperatures for these fuels is narrow, even though the boiling point range is wide, providing guidance for determining evaporation conditions. The average boiling point and T_c of HVO:C_{15}-C_{18}/isododecane are lower compared to other HVO surrogate fuels while P_c is higher. This suggests that HVO:C_{15}-C_{18}/isododecane is likely to exhibit better spray and evaporation behaviors compared to other HVO surrogate fuels under the same conditions. The lower boiling point and critical temperature contribute to these enhanced spray and evaporation behaviors.

Table 4. Properties of HVO fuels and diesel

Properties	Density at 15°C g/mL	Viscosity at 40°C mm^2/s	Surface tension at 20°C mN/m	Boiling point rage (T_b) °C	T_c K	P_c bar
Diesel (D2)	0.842[a]	2.84[a]	28	174-360	726[a]	20.90[a]
Algal HVO	0.772	2.3	24.6 ± 0.3	180-320	-	-
HVO:C_{15}-C_{18}	0.7768	3.23	-	271-317 (299.23[b])	730[c]	12.90[c]
HVO:C_{15}-C_{18}/isooctane	0.7752	3.13	24.5	99-317 (294.64[b])	726[c]	13.05[c]
HVO:C_{15}-C_{18}/isododecane	0.7684	2.37	24.1 ± 0.4	178-317 (261.35[b])	701[c*]	14.45[c]

a: values obtained from Ref [31]
b: average boiling point calculated based on the mass fraction using Eq. (3.3)
c: value calculated based on Riazi-Daubert Correlation in Ref [25]
*: critical temperature calculated based on T_b and SG obtained from Eq. (3.3)

188 2.4 Experimental apparatus and test conditions

189 The schematic of the experimental apparatus for droplet evaporation test is shown in Fig.
190 2. The pressure vessel (inner diameter: 100 mm; inner height: 229 mm) was made of extra
191 super Duralumin (JIS A7075). The top cover of the vessel was equipped with a temperature-
192 controlled hot chamber (upper) and droplet generation and sliding mechanisms (lower), as
193 shown in Fig. 2a. The whole top cover assembly was attached to the pressure vessel, thus
194 achieving the same pressure for the droplet generation part and the hot chamber part. The
195 ambient temperature (T_{amb}) inside the hot chamber was arbitrarily controlled by a thermal
196 control unit while ambient pressure (P_{amb}) was controlled by regulating the pressure inlet valve
197 connected to the high-pressure N_2 cylinder. Before conducting experiments, the vessel was
198 vacuumed and filled with N_2 to observe pure evaporation without a combustion reaction. Then,
199 a microflow pump was used to deliver fuel to the tip of the glass needle (outer diameter: 40
200 μm) of the droplet generator. Inside the pressure vessel, the fuel droplet with a diameter in the
201 range of 500±15% μm was then suspended onto the intersection point of two Al_2O_3/SiO_2 fibers
202 with a 7 μm diameter as indicated in Fig. 2b. A charge-couple device (CCD) video camera was
203 used to monitor the droplet generation process. Finally, after droplet generation, the glass
204 needle was evacuated in preparation for the droplet insertion into the hot chamber via an open
205 entrance for the droplet suspender holder. The area of the open entrance is small compared to
206 the bottom surface of the hot chamber so that the heat escape from the hot chamber is as small
207 as possible. The fuel droplet elevator was equipped with a linear slider-crank mechanism to
208 reduce the impact on the suspended droplet during the droplet insertion process. The droplet
209 insertion time to the hot chamber was 0.26 s, corresponding to the traveling distance of 60 mm.
210 Two high-speed cameras (DITECT, HAS-X) were used to observe the droplet diameter change
211 during both the droplet generation process and the evaporation process. The images of an
212 evaporating droplet were captured by the high-speed cameras using the shadowgraph method

and the recording rate varied between 10 to 250 images/s. Thus, the total number of recorded images in each test was above 130, which was sufficient to calculate the droplet lifetime and instantaneous evaporation coefficient. The evaporation tests were conducted at various temperatures (573-873 K) and pressures (0.1-2.0 MPa).

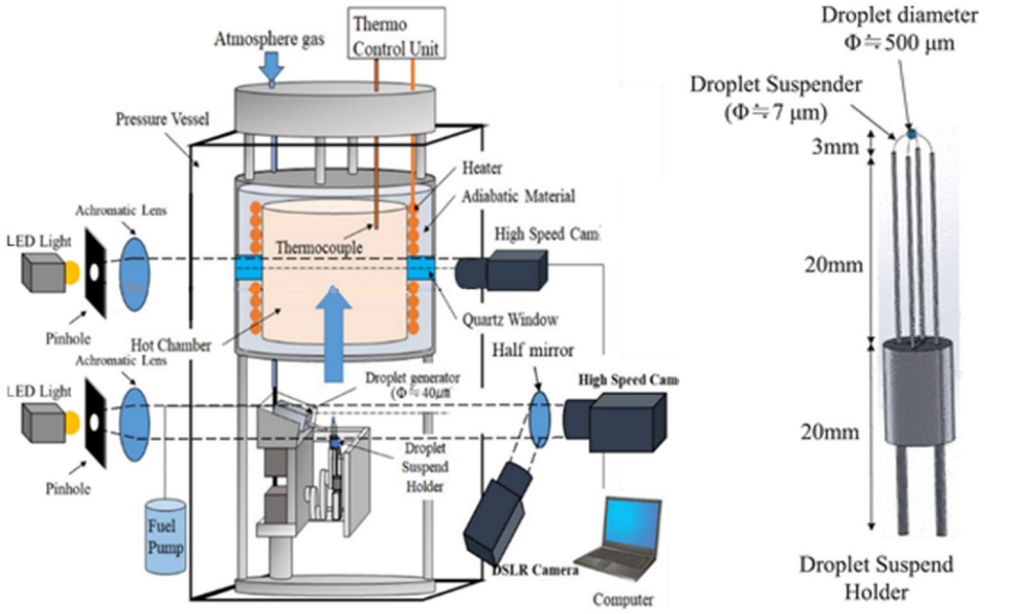

(a) Droplet evaporation experimental setup (b) Schematic of droplet suspender

Fig. 2. Schematic of droplet evaporation experimental apparatus[32].

Figure 3 shows the details of the image analysis of this experiment. The droplet diameter (D) was measured by an in-house computer-aided image analyzer. Each digital image of a fuel droplet was separated into horizontal line portions with a vertical thickness of 2 pixels. The average horizontal intensity profiles were computed for each section. The edge of a droplet was defined as the greatest distance from the suspender at which the gradient of light intensity is maximum. Then, the detected droplet edges were used to calculate the droplet volume by an ellipsoidal approximation. Finally, the droplet diameter was defined as the diameter of a sphere with the same volume. The measurement limit for the droplet diameter was under 0.078 mm, which corresponded to $D^2/D_0^2 = 0.025$. The droplet diameter before and after droplet insertion into the hot chamber was measured and compared to observe the impact of the irregular shape

of the droplet. The average error of diameter difference is below 5%[32]. The pressure and temperature data were recorded to evaluate the measurement uncertainty of the experiment. The accuracy of the temperature and pressure sensors are ±0.4% and ±0.5% respectively while the measurement uncertainties for temperature and pressure are consistently less than ±0.5% and ±1.5% respectively, underscoring the precision reliability of the experiment measurement.

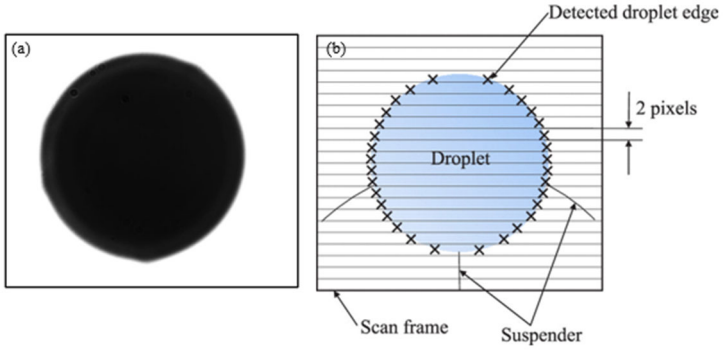

Fig. 3. Schematics of the image processing method, (a) digital image and (b) processed image.

Figure 4. shows the definitions of evaporation periods. The moment when the fuel droplet was delivered to the hot chamber is defined as time=0 while D_0 is the initial droplet diameter when time=0. The droplet diameter and droplet lifetime were normalized by the initial diameter squared (D_0^2) to reduce initial droplet diameter dispersion. Therefore, the horizontal and vertical axes represented the normalized droplet lifetime (t/D_0^2) and the normalized droplet diameter (D^2/D_0^2), respectively. The definitions of periods were divided into a pre-evaporation period and a droplet evaporation period. During the droplet generation process, some lighter components in the fuel were affected by the droplet generation part temperature (T_{dg}). Thus, D^2/D_0^2 decreased toward unity before the droplet was delivered to the hot chamber. For example, at T_{amb} = 773 K and P_{amb} = 0.1 MPa, the D^2/D_0^2 for HVO:C_{15}-C_{18}/isododecane decreased toward unity while that for HVO:C_{15}-C_{18}/n-dodecane remained unchanged during the whole droplet generation process. This was because T_{dg} = 98-110℃ was closer to the boiling point of isododecane (T_b = 177.8℃), causing pre-evaporation of isododecane. The

definitions of periods during the droplet evaporation process were described as follows based on the periods defined by Hashimoto et al. [27].

- Droplet expansion period was the initial duration when the droplet absorbed heat and raised its temperature, yielding maximum droplet diameter due to thermal expansion.
- The initial heating period (t_i/D_0^2) was defined as the duration between the time when the droplet was inserted into the hot chamber and the time when the droplet diameter equaled the initial droplet diameter.
- The period of 95% volume lifetime ($t_{v0.95}/D_0^2$) was defined as the period between the time when a droplet is inserted in the hot chamber and the time when droplet volume remained 5% of the initial volume, equivalent to D^2/D_0^2 = 0.136, where the exact time of complete evaporation could not be found.
- The main evaporation period (t_{evap}/D_0^2) was defined to examine the instantaneous evaporation coefficient (K_{inst}). This period is defined as the duration starting from the end of the initial heating period until the intersection between the axis corresponding to D^2/D_0^2 = 0 and the line extrapolated from D^2/D_0^2 =0.3 to D^2/D_0^2 = 0.136.

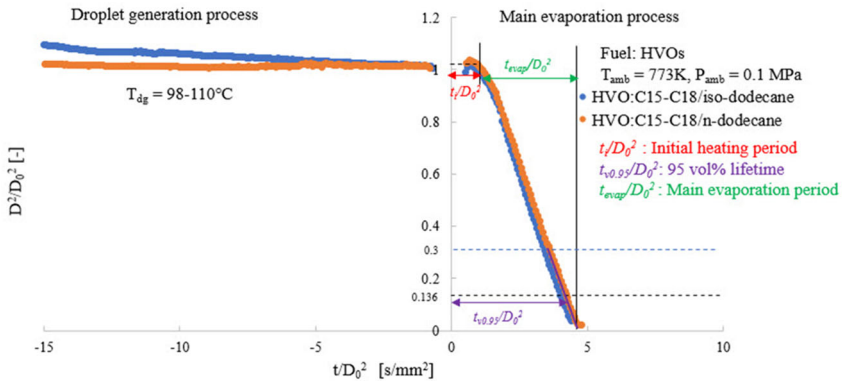

Fig. 4. Definitions of evaporation periods.

3. Results and Discussion

Normalized droplet lifetime (t/D_0^2) and instantaneous evaporation coefficient (K_{inst}) of hydrocarbons, HVO surrogate fuels, and diesel are presented accordingly. Moreover, the effect of pressures and temperatures on evaporation characteristics is discussed in detail. Finally, the effect of branching alkanes on evaporation is highlighted. All experimental data related to this study are given in the Supporting Information. Five experiments were conducted under the same conditions for all fuels to ensure the reliability and consistency of the experimental data. Notably, the standard deviation of the experimental results derived from the five experiments is minimal, measuring less than 1% (Appendix C). This signifies high precision and repeatability in the obtained experimental data.

3.1 Droplet evaporation characteristics

This section presents the droplet evaporation characteristics of hydrocarbons, HVO surrogate fuels, and diesel. The definitions of periods defined in this study are used to describe the history of D^2/D_0^2 change during droplet generation and evaporation processes. During the droplet evaporation experiment, the bubble formation and evolution were not observed inside the droplet and the micro-explosion phenomenon did not appear under all temperature and pressure conditions.

3.1.1 Droplet evaporation characteristics of pure hydrocarbons

Figure 5 shows the normalized droplet diameter (D^2/D_0^2) history for pure hydrocarbons at T_{amb} = 573 K, P_{amb} = 0.1 MPa during the whole evaporation process. The evaporation test with n-$C_{18}H_{38}$ cannot be performed because its melting point is higher than the controlled ambient temperature in the experimental room while the evaporation test with n-$C_{12}H_{26}$ is conducted instead of iso-$C_{12}H_{26}$ to avoid pre-evaporation. During the droplet generation process, the change of D^2/D_0^2 histories remains unity, which indicates that the droplet evaporation rate is

very low at droplet generation part temperature (T_{dg}). This is because T_{dg} = 50-60°C @ T_{amb} = 573 K is much lower than the initial boiling point of tested fuels (T_b > 231°C). During the evaporation process, the initial heating period is clearly observed for all fuels because the droplet diameter initially increases due to thermal expansion. Then, the droplet diameter decreases monotonically during the main evaporation period, following the D^2 law. The initial increase in the droplet diameter was also observed in other studies by Hashimoto et al. [27], Daho et al. [16], and Morin et al. [33]. It is observed that lighter components exhibit shorter droplet lifetimes than heavier components. The normalized droplet lifetimes (t/D_0^2) for n-$C_{12}H_{26}$, n-$C_{15}H_{32}$, n-$C_{16}H_{34}$, and n-$C_{17}H_{36}$ are 10.62, 14.79, 16.29, and 18.17 (s/mm^2), respectively. This trend matches the order of the lower boiling point of fuels. For example, n-$C_{12}H_{26}$ with a lower boiling point has a shorter initial heating period and droplet lifetime than n-$C_{17}H_{36}$ with a higher boiling point.

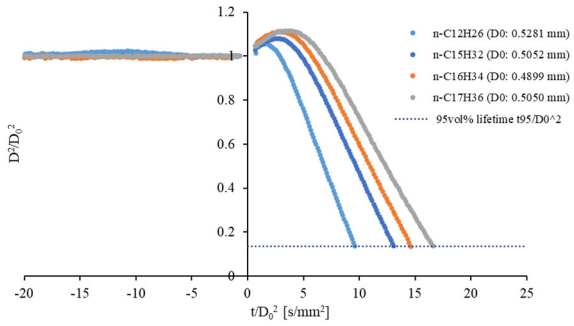

Fig. 5. History of normalized D^2 for pure hydrocarbons during the whole evaporation process.

The instantaneous evaporation coefficient (K_{inst}) for pure hydrocarbons at T_{amb}=573 K and P_{amb}=0.1 MPa is indicated in Fig. 6. The fluctuation in the K_{inst} is caused by the image analysis error. Similarly, the order of K_{inst} matches the order of the boiling point of each fuel. The average values of K_{inst} for n-$C_{12}H_{32}$, n-$C_{15}H_{32}$, n-$C_{16}H_{34}$, and n-$C_{17}H_{36}$ are 0.1316, 0.1058, 0.1019, and 0.0889 mm^2/s, respectively. The evaporation rate of heavier components is lower than that of lighter components due to the higher boiling point, which generally leads to a

longer initial heating period and results in a decreased evaporation rate. This trend was also observed in a previous study by Naito et al. [32]. They conducted a droplet evaporation experiment with multicomponent surrogate fuels and found that the K_{inst} of fuels matched the order of the higher boiling point. The lower K_{inst} values correspond to the higher boiling points. The K_{inst} of each hydrocarbon slightly decreases during the main evaporation. This is because the rate of decrease in D^2/D_0^2 shown in Fig. 5 is not constant as time progresses.

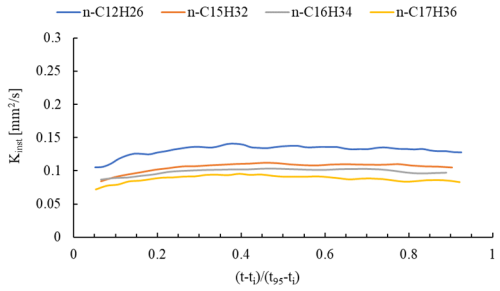

Fig. 6. Instantaneous evaporation coefficient (K_{int}) for pure hydrocarbons.

3.1.2 Droplet evaporation characteristics of hydrotreated vegetable oil

Figure 7 illustrates the D^2/D_0^2 histories for HVO surrogate fuels and diesel during the whole evaporation process at T_{amb} = 573-873 K and P_{amb} = 0.1 MPa. It shall be noted that the t/D_0^2 during droplet generation is shortened accordingly to enhance the visibility of the droplet lifetime during the evaporation process. It is observed that the D^2/D_0^2 for diesel, HVO:C_{15}-C_{18}/isododecane, and HVO:C_{15}-C_{18}/isooctane decreases toward unity during the droplet generation process as shown in Fig. 7a-7d. This is because T_{dg} = 50-130°C @ T_{amb} = 573-873 K is high enough to make some portion of lighter components in diesel, isododecane, and isooctane evaporated. Droplet lifetimes for all fuels significantly decrease with increasing ambient temperature. The difference in t/D_0^2 becomes relatively small as temperature increases (Fig. 7b-7d). Under all temperatures, HVO surrogate fuels have shorter droplet lifetimes compared to diesel. This is expected because the mass fraction of components with low boiling points for HVO surrogate fuels is higher than that for diesel. In Fig. 7a, it is observed that

diesel preferentially evaporates first due to light-end components with lower boiling points as indicated by a shorter initial heating period compared to HVO:C_{15}-C_{18} and HVO:C_{15}-C_{18}/isooctane. However, diesel has a longer droplet lifetime due to the heavy-end components with higher final boiling points, which reduces the evaporation rate during the latter evaporation process[27]. Among HVO surrogate fuels, HVO:C_{15}-C_{18}/isododecane has the shortest droplet lifetime because adding isododecane lowers the boiling point of the mixture and shortens the initial heating period. Moreover, as shown in Fig. 7a and 7b, two-stage evaporation can be observed, during which the evaporation rate is dominantly controlled by the lighter component and the heavier components. Isododecane preferentially evaporates faster in the early stage before the heavier components start to evaporate in the latter stage. As temperature increases, the two-stage evaporation degrades and disappears at 873 K. This is because isododecane (T_b =177.8℃) seems to mostly evaporate during the droplet generation process under T_{dg} = 120-130℃ @ T_{amb} = 873 K. As shown in Fig. 7d, the D^2/D_0^2 of HVO:C_{15}-C_{18}/isododecane is steeper during the droplet generation process, whereas t/D_0^2 becomes slightly longer compared to that of HVO:C_{15}-C_{18} during the evaporation process. Ghassemi et al. conducted a droplet evaporation experiment with a 50% heptane+50% hexadecane mixture at T_{amb} =400-700℃ and found that the two-stage evaporation clearly appeared at 400℃, and eventually became less visible at 700℃ [34]. Similarly, Long et al. established a vaporization model for multi-component fuels and validated the model using the experimental data obtained by Ghassemi et al[34]. The model agreed well with the experiment and the two-stage evaporation was also observed [35]. Overall, it is concluded that the evaporation of HVO:C_{15}-C_{18}/isododecane is more promoted under actual engine operating conditions, where fuel droplets expose to high temperatures quickly after fuel injection.

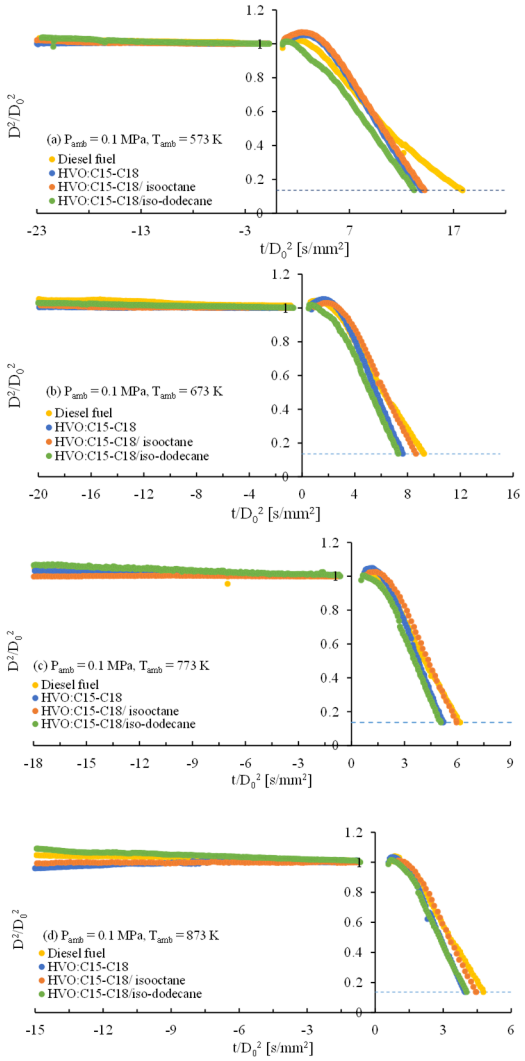

Fig. 7. History of normalized D^2 for HVO surrogate fuels and diesel during the whole evaporation process.

The K_{inst} for HVO surrogate fuels and diesel at T_{amb} = 573-873 K and P_{amb} = 0.1 MPa are shown in Fig. 8. In Ref [27], it is reported that K_{inst} strongly depends on T_{amb}. Generally, K_{inst} increases with increasing ambient temperature because higher temperature enhances the mass and heat transfer between the droplet core and ambient gas, thus increasing the evaporation rate[36,37]. The K_{inst} of HVO surrogate fuels is found to be higher than that of diesel. The K_{inst} of HVO surrogate fuels gradually increases and then remains almost constant during the latter evaporation process while the K_{inst} of diesel decreases monotonically with time because diesel contains a wide range of boiling points compared to HVO surrogate fuels (Fig. 8a and 8b).

The components with a lower boiling point evaporate in the early stage while the components with a higher boiling point evaporate later[27]. As temperature increases, the slope of K_{inst} for diesel is raised because both light-end and heavy-end components evaporate simultaneously and enhance the evaporation rate due to more heat conduction from the ambient gas into the droplet core (Fig. 8c and 8d). In Fig. 8a and 8b, HVO:C_{15}-C_{18}/isododecane exhibits much lower evaporation rates during the early stage despite a lower boiling point, but gradually increases toward a similar level, compared to HVO:C_{15}-C_{18} and HVO:C_{15}-C_{18}/isooctane. This is because the pre-evaporation of isododecane causes an impending effect on the evaporation rate meanwhile adding isododecane reduces the initial heating period and lowers droplet surface temperature due to lower thermal conductivity and latent heat of vaporization, thus producing a lower evaporation rate during the early stage[21,34]. Subsequently, the droplet temperature increases because the light components evaporate completely before the latter stage of evaporation, thus resulting in an increased evaporation rate during the latter stage. However, as temperature increases up to 873 K, the evaporation rate of HVO:C_{15}-C_{18}/isododecane is enhanced throughout the evaporation process (Fig. 8d) because all components evaporate simultaneously due to a strong heat transfer [36]. The K_{inst} for HVO:C_{15}-C_{18}/isododecane and HVO:C_{15}-C_{18}/isooctane also shows lower trends compared to that for HVO:C_{15}-C_{18} during the remaining evaporation process. The reason for this is explained in section 3.2. In Ref[34], the binary droplet evaporation at elevated pressure and temperature was conducted. It was found that the evaporation rate of 50% heptane + 50% hexadecane was lower than that of pure hexadecane under various temperatures and pressures. It was justified that the presence of heptane vapor decreased the total heat transfer from ambient gas to the droplet.

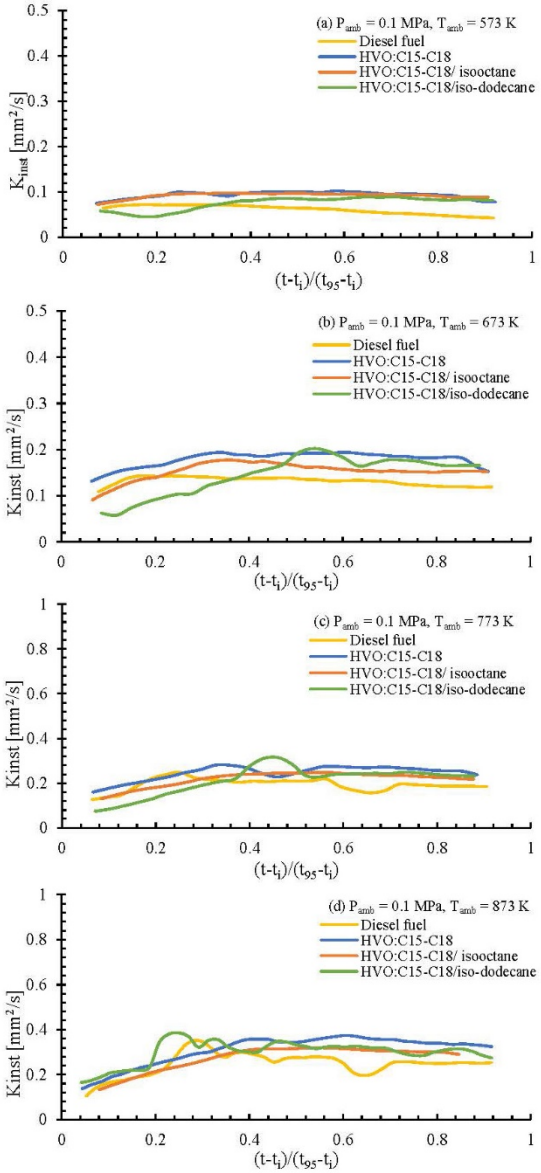

389

390 Fig. 8. Instantaneous evaporation coefficient (K_{int}) for HVO surrogate fuels and diesel.

391 3.2 Effect of ambient temperature on evaporation characteristics

392 Figure 9. illustrates the normalized 95 vol% lifetimes (t_{95}/D_0^2) for HVO surrogate fuels and
393 diesel as a function of ambient temperature. Each plot represents the average value for five
394 experiments conducted under the same conditions. The error bars of each plot indicate the
395 minimum and maximum values from the five experiments. Under all ambient pressures, t_{95}/D_0^2
396 decreases with increasing temperatures. HVO surrogate fuels exhibit shorter droplet lifetime
397 compared to diesel. In Fig. 9a, despite having a slightly lower boiling point, HVO:C15-

18/isooctane has longer droplet lifetimes than HVO:C_{15}-C_{18}, especially at higher temperatures. At T_{amb} = 873 K, the t_{95}/D_0^2 for HVO:C_{15}-C_{18}/isododecane is slightly longer than that for HVO:C_{15}-C_{18}, which was not expected. This is because isooctane (T_b = 99.2℃) and isododecane (T_b = 177.8℃) evaporate under T_{dg} = 50-130℃ @T_{amb}=573-873K during the droplet generation process, especially at low pressure under which diffusion resistance is less. This allows light-end components to evaporate faster, which eventually reduces the influence of boiling point on the evaporation rate during the evaporation process. Considering the pre-evaporation, the influence of boiling point for both HVO:C_{15}-C_{18}/isododecane and HVO:C_{15}-C_{18} on the evaporation rate may become almost similar during the evaporation process. In this case, according to the well-known equation of D^2 law described as $dD^2/dt = -[8\lambda_g/(\rho_l C_{pg})] ln(B+1)$ in Ref [27], the ratio of thermal conductivity and specific heat of gas (λ_g/C_{pg}) greatly affect the evaporation characteristics. Therefore, HVO:C_{15}-C_{18} consisting of a higher mass fraction of components with higher λ/C_p (Table 3) gains more heat transfer into the droplet. Consequently, evaporation of HVO:C_{15}-C_{18} droplets takes place at a faster rate than that of HVO:C_{15}-C_{18}/isooctane and HVO:C_{15}-C_{18}/isododecane, thus decreasing droplet lifetime. Moreover, based on equations (48) and (51) described in Ref [21], both heating and evaporation times are shortened under the increment of thermodynamic properties (λ_g and C_{pg}). However, this trend is weakened at higher ambient pressures, especially for HVO:C_{15}-C_{18}/isododecane because increasing pressure slows down the evaporation of isooctane and isododecane during the droplet generation process. As shown in Fig. 9b-9e, the trend line of t_{95}/D_0^2 for HVO:C_{15}-C_{18}/isododecane detaches itself from that of HVO:C_{15}-C_{18}, especially at low temperatures because the presence of isododecane remains in the mixture until the main evaporation process, thus reducing droplet lifetime. Considering the effect of T_{dg} at higher ambient pressures, the t_{95}/D_0^2 of HVO with and without isooctane is almost the same under all ambient temperatures and pressures from 1.0-2.0 MPa (Fig. 9c-9e) because HVO:C_{15}-C_{18}/isooctane (2.23%) and

HVO:C_{15}-C_{18} may have almost identical properties while the combined effect of T_b and λ/C_p on evaporation rate becomes similar for both fuels.

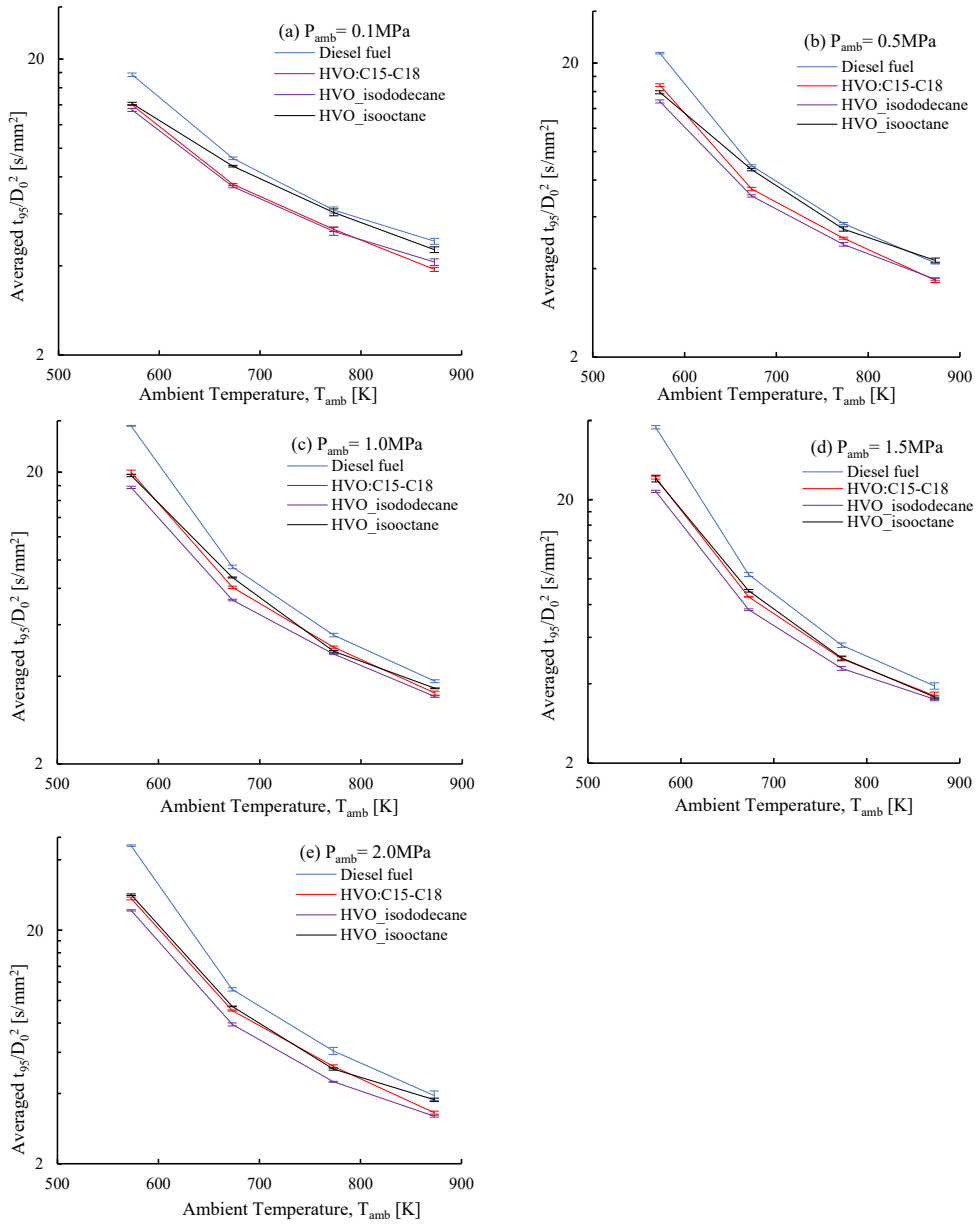

Fig. 9. Normalized 95 vol% lifetimes (t_{95}/D_0^2) for HVO surrogate fuels and diesel as a function of ambient temperature.

3.3 Effect of ambient pressure on evaporation characteristics

The effect of ambient pressure on droplet evaporation characteristics for HVO:C_{15}-C_{18}/isododecane only is shown in Fig. 10 since all fuels have a similar tendency. It is observed that the effect of pressure on droplet lifetime relies on temperatures. The ambient conditions

significantly affect phase equilibrium between fuel vapor and ambient gas at the droplet surface and droplet surface temperature[37]. Generally, increasing pressure always results in a longer initial heating period at various temperatures because droplet evaporation is suppressed by higher boiling points. Initially, the heat from ambient gas is not used for evaporation, but for raising the droplet temperature to the equilibrium temperature[37,38]. In Fig. 10a, at T_{amb} = 573 K, droplet lifetime increases with increasing pressure because higher pressure exerts on the droplet surface and increases diffusion resistance. The increase in pressure leads to a decrease in the vapor pressure faction to the ambient pressure, which results in a lower vapor mass fraction and eventually reduces the evaporation rate [37]. As the temperature increases, the droplet lifetime decreases or increases according to pressure. For example, at T_{amb} = 673 K, increasing pressure up to 0.5 MPa shortens the droplet lifetime while further increasing pressure prolongs the droplet lifetime (Fig. 10b). This is related to competition between gasification and diffusion resistance. At high temperatures, gasification and diffusion can be promoted simultaneously with the increase in pressure at low and moderate pressure conditions because droplet surface temperature reaches a certain point at which the increased saturated vapor pressure overcomes the diffusion resistance and increases the evaporation rate[37]. However, when the pressure is further increased, diffusion resistance overcomes the promoted gasification, thus reducing the evaporation rate. At T_{amb} =773-873 K, the higher the temperatures and pressures, the shorter droplet lifetimes are obtained as shown in Fig. 10c and 10d. Despite longer initial heating periods, droplet lifetime decreases with increasing pressure because gasification and diffusion capability are enhanced simultaneously under all pressures, thus further increasing the saturated vapor pressure and evaporation rate. This trend was also observed in a numerical study on heptane and dodecane evaporation done by Kitano et al.[38] and on ethanol evaporation by Pinheiro et al.[37] and Yi et al.[39]. Droplet lifetime increased with increasing ambient pressure at low ambient temperatures but decreased at high ambient

temperatures. For more comprehension, the effect of pressure on the K_{inst} is also discussed in detail in Fig. 11.

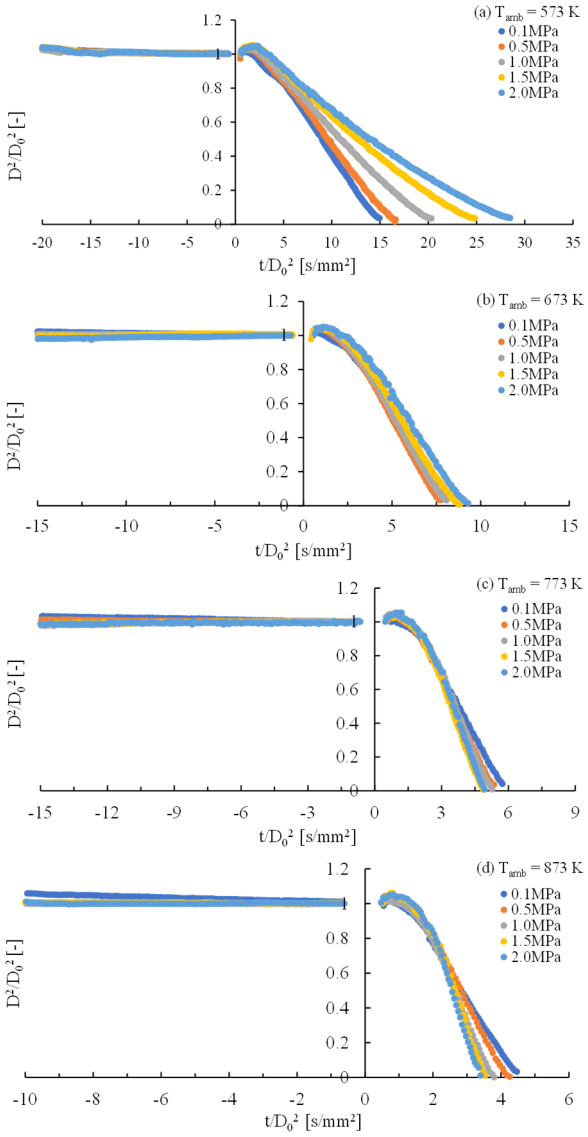

Fig. 10. Histories of normalized droplet lifetime (t/D_0^2) for HVO:C_{15}-C_{18}/iso-dodecane at different temperatures and pressures.

Figure 11 shows the effect of pressure on K_{inst} for HVO:C_{15}-C_{18}/iso-dodecane at different temperatures. Notably, the fluctuation in K_{inst} is quite strong in some cases, particularly under high-temperature and pressure conditions. This variation can be attributed to image analysis errors arising from the presence of fuel vapor surrounding the droplet. Since the effect of

pressure on K_{inst} is complicated and relies on temperatures, it is important to introduce the critical temperature of HVO:C_{15}-C_{18}/iso-dodecane (T_c =701 K) in the discussion. In Fig. 11a, at T_{amb} =573 K < T_c =701 K, the K_{inst} decreases with increasing pressure because pressure acting on the droplet surface suppresses the evaporation, which decreases the vapor mass fraction at the droplet surface and the Spalding mass transfer number, $B_M=(Y_{vs}-Y_{vg})/(1-Y_{vs})$, and consequently reduces the evaporation rate [35,37]. Specifically, at P_{amb}=0.1 MPa, the initial K_{inst} is degraded due to a shorter initial heating period which reduces the initial droplet surface temperature. At moderate pressure, the evaporation is suppressed, and the initial heating period is prolonged, causing the initial K_{inst} to increase due to higher droplet surface temperature. Finally, the initial K_{inst} will determine the subsequent evaporation rate according to the resulting temperature gradient between the droplet surface and ambient gas. However, at T_{amb} = 773-873 K > T_c = 701 K, this trend is not followed. Increasing pressure generally increases the evaporation rate (Fig. 11c and 11d) because there is an increase in vapor mass fraction and Spalding mass transfer number due to the increased droplet surface temperature[37]. Moreover, increasing temperature and pressure leads to higher conduction heat flux and reduced latent heat of vaporization[35]. Therefore, the evaporation rate for both light- and heavy-end components increases simultaneously, and both components coexist throughout the evaporation process. At T_{amb} = 673 K ~ T_c = 701 K, it is observed that the evaporation rate increases or decreases according to ambient pressure. The difference between K_{inst} is narrow, as indicated in Fig. 11b. This implies that there is an ambient temperature at which the K_{inst} becomes almost independent of pressure. This threshold temperature is found to be near the critical temperature of the fuel in this study. This phenomenon can be further clarified in Fig.12.

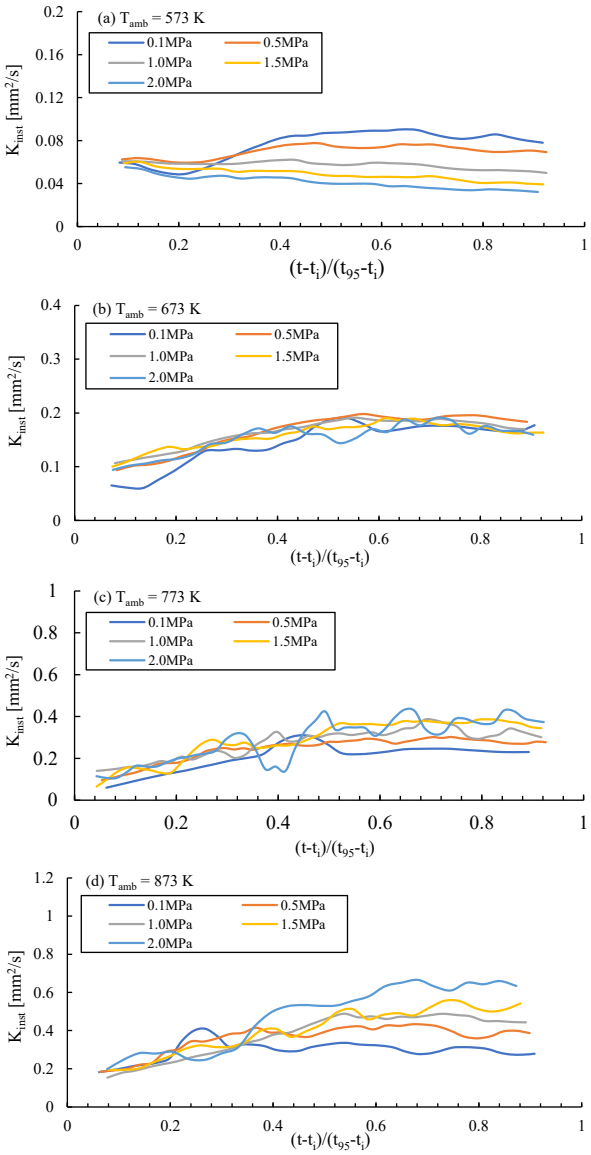

Fig. 11. Instantaneous evaporation coefficient (K_{inst}) for HVO:C_{15}-C_{18}/iso-dodecane at different pressures and temperatures.

Critical point (T_c, P_c) plays a significant role in determining the effect of ambient pressure on evaporation characteristics. It denotes the conditions at which a substance undergoes a critical phase transition from liquid to vapor, a phenomenon crucial for understanding evaporation characteristics. Despite its significance, calculating the critical temperature and pressure for the hydrocarbon mixture is challenging. In section 2.2, we discuss the use of correlations to approximate Tc and Pc, recognizing the complexity of determining these values

precisely. Figure 12 illustrates the coupling effect of ambient pressure and temperature on t_{95}/D_0^2 for diesel and HVO:C_{15}-C_{18}/isododecane. The data of t_{95}/D_0^2 for both fuels are given in Appendix C. The evaporation characteristics can be determined under three main conditions such as subcritical, transcritical, and supercritical conditions. At subcritical conditions ($T_{amb} < T_c$), where the ambient temperature is below the critical temperature, t_{95}/D_0^2 increases with increasing pressure because the evaporation rate decreases due to high diffusion resistance at the droplet surface. The evaporation rate monotonically decreases as light-end components are consumed, respectively [37,38]. Conversely, under supercritical conditions ($T_{amb} > T_c$), where ambient temperature surpasses the critical temperature, increasing pressure shortens the droplet lifetime due to an increase in droplet surface temperature. The saturated vapor pressure increases with increasing temperature while the heat conduction coefficient increases with increasing pressure due to promoted natural convection, thus enhancing the heat transfer and evaporation rate of all species simultaneously[37,40]. It is noteworthy that even when the ambient pressure exceeds the critical pressure, the droplet surface does not reach a supercritical state because the temperature of the droplet surface cannot reach the supercritical temperature due to latent heat, except in cases of significantly higher ambient pressure ($P_{amb} >> P_c$). Between subcritical and supercritical regions, there is a transcritical condition ($T_{amb} \sim T_c$) at which the droplet lifetime becomes almost independent of pressure. As indicated in Fig. 12a and 12b, the variation in t_{95}/D_0^2 is very narrow regardless of applied pressures at T_{amb} = 700-720 K~ T_c =726 K for diesel and T_{amb} = 680-700 K~ T_c =701 K for HVO:C_{15}-C_{18}/isododecane. This is attributed to a balance of the increase and decrease of the droplet evaporation rate in higher ambient pressure conditions. Nomura et al.'s study on n-heptane droplet evaporation in high-pressure microgravity conditions supports this observation, with a consistent slope of droplet lifetime[19]. The transition temperature, where droplet lifetime becomes almost independent of pressure, was 480 K for h-heptane, closely aligning with its critical temperature

(T_c=540 K). This observation suggests a phenomenon where a transition temperature, approximately near the critical temperature, signifies a point at which droplet lifetime becomes pressure-independent, acknowledging the inherent challenges in precisely determining this critical transition point.

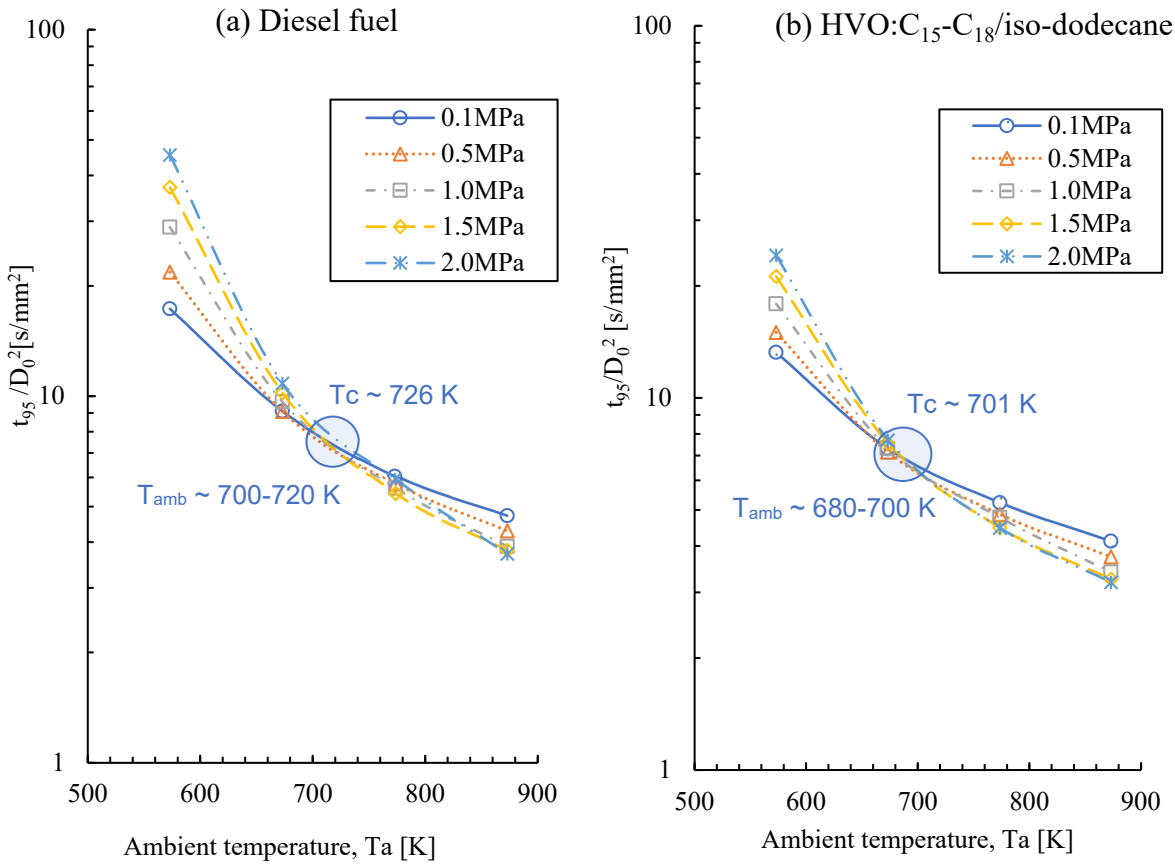

Fig. 12. Variation of t_{95}/D_0^2 for (a) diesel and (b) HVO:C_{15}-C_{18}/iso-dodecane with ambient temperatures and pressures.

3.4 Effect of iso-alkane on evaporation characteristics

The effect of iso-alkane on evaporation characteristics is shown in Fig. 13. Compared to n-dodecane, the addition of isododecane enhances the evaporation of the HVO surrogate mixture under all ambient conditions. This is expected because isododecane is a branching alkane with a lower boiling point compared to n-dodecane. Generally, branching components have smaller contact areas of interaction between two molecules and lead to weaker intermolecular Van der

Waals force, which can be overcome at a relatively lower temperature. Hence, the boiling point of HVO/isododecane is lower than that of HVO/n-dodecane. It is observed that the difference between droplet lifetimes of HVO/n-dodecane and HVO/isododecane becomes larger with increasing pressure, especially at low ambient temperatures because the evaporation of isododecane (T_b = 177.8°C) is suppressed and is not much affected by the droplet generation part temperature (T_{dg} = 50-60°C @ T_{amb}=573K). The difference becomes much smaller at higher temperatures because more isododecane is evaporated before the droplet is delivered to the hot chamber. This trend is obvious at T_{amb} = 873 K. Insignificant difference is observed between the evaporation of these two fuels because isododecane mostly evaporates during the droplet generation process due to higher droplet generation temperature (T_{dg} = 120-130°C @ T_{amb}=873K). Therefore, it can be concluded that adding a considerable amount of iso-alkane enhances the evaporation characteristics of HVO over a wide range of ambient conditions.

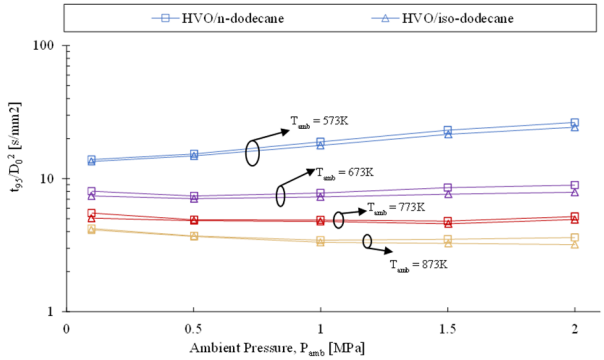

Fig. 13. Comparison of t_{95}/D_0^2 between n-alkane and iso-alkane addition.

4. Conclusion

The evaporation characteristics of HVO surrogate fuels under high ambient conditions are thoroughly investigated. Thermodynamic and physical properties, droplet lifetime, and instantaneous evaporation coefficient are discussed. The main findings are as follows:

- All HVO surrogate fuels exhibit lower density, surface tension, and boiling point, thus enhancing evaporation rate and reducing droplet lifetime while diesel has a lower

evaporation rate and longer droplet lifetime due to its higher final boiling points. Among HVO surrogate fuels, HVO:C_{15}-C_{18}/isododecane has the shortest droplet lifetime because adding isododecane reduces the initial heating period due to its lower boiling point. Moreover, HVO:C_{15}-C_{18}/isododecane has a lower critical temperature (T_c) and higher critical pressure (P_c) than other fuels, thus allowing broader efficient evaporating conditions. The evaporation rate of HVO surrogate fuels depends on not only the boiling point but also fuel composition and thermodynamic properties such as thermal conductivity, latent heat of vaporization, and specific heat.

- Temperature and pressure have a strong coupling effect on evaporation characteristics. The evaporation rate increases with increasing temperature due to high heat transfer from the ambient gas to the droplet, thus reducing droplet lifetime. The effect of ambient pressure on evaporation characteristics relies on ambient temperature. At $T_{amb} < T_c$, droplet lifetime increases with increasing pressure due to the reduction in evaporation rate. However, at $T_{amb} > T_c$, increasing pressure increases the evaporation rate, thus reducing droplet lifetime while at $T_{amb} \sim T_c$, increasing pressure has no significant effect on droplet lifetime.

These results are significant for optimizing the combustion of heavy-duty engines operated under various in-cylinder conditions. A multi-component droplet evaporation model should be developed to investigate evaporation characteristics at supercritical conditions.

Acknowledgments

This work was partly supported by JSPS KAKENHI Grant Numbers JP20KK0319.

Reference

[1] IEA. Global energy-related CO2 emissions by sector. IEA 2022.

[2] Di Blasio G, Ianniello R, Beatrice C. Hydrotreated vegetable oil as enabler for high-efficient and ultra-low emission vehicles in the view of 2030 targets. Fuel 2022;310:122206. https://doi.org/10.1016/j.fuel.2021.122206.

[3] Ushakov S, Lefebvre N. Assessment of Hydrotreated Vegetable Oil (HVO) Applicability as an Alternative Marine Fuel Based on Its Performance and Emissions Characteristics. SAE Int J Fuels Lubr 2019;12:04-12-02–0007. https://doi.org/10.4271/04-12-02-0007.

[4] Hunicz J, Mikulski M, Shukla PC, Gęca MS. Partially premixed combustion of hydrotreated vegetable oil in a diesel engine: Sensitivity to boost and exhaust gas recirculation. Fuel 2022;307:121910. https://doi.org/10.1016/j.fuel.2021.121910.

[5] Kim D, Kim S, Oh S, No S-Y. Engine performance and emission characteristics of hydrotreated vegetable oil in light duty diesel engines. Fuel 2014;125:36–43. https://doi.org/10.1016/j.fuel.2014.01.089.

[6] Bjørgen KOP, Emberson DR, Løvås T. Combustion and soot characteristics of hydrotreated vegetable oil compression-ignited spray flames. Fuel 2020;266:116942. https://doi.org/10.1016/j.fuel.2019.116942.

[7] Lapuerta M, Villajos M, Agudelo JR, Boehman AL. Key properties and blending strategies of hydrotreated vegetable oil as biofuel for diesel engines. Fuel Processing Technology 2011;92:2406–11. https://doi.org/10.1016/j.fuproc.2011.09.003.

[8] Neste. Neste Renewable Diesel Handbook. Neste Corporation; 2020.

[9] Murtonen T, Aakko-Saksa P, Kuronen M, Mikkonen S, Lehtoranta K. Emissions with Heavy-duty Diesel Engines and Vehicles using FAME, HVO and GTL Fuels with and without DOC+POC Aftertreatment. SAE Int J Fuels Lubr 2009;2:2009-01–2693. https://doi.org/10.4271/2009-01-2693.

[10] Han J, Wang Y, Somers LMT, van de Beld B. Ignition and combustion characteristics of hydrotreated pyrolysis oil in a combustion research unit. Fuel 2022;316:123419. https://doi.org/10.1016/j.fuel.2022.123419.

[11] Li Y, Xu H, Cracknell R, Head R, Shuai S. An experimental investigation into combustion characteristics of HVO compared with TME and ULSD at varied blend ratios. Fuel 2019;255:115757. https://doi.org/10.1016/j.fuel.2019.115757.

[12] Hulkkonen T, Hillamo H, Sarjovaara T, Larmi M. Experimental Study of Spray Characteristics between Hydrotreated Vegetable Oil (HVO) and Crude Oil Based EN 590 Diesel Fuel, SAE technical paper; 2011. https://doi.org/10.4271/2011-24-0042.

[13] Bohl T, Smallbone A, Tian G, Roskilly AP. Particulate number and NO trade-off comparisons between HVO and mineral diesel in HD applications. Fuel 2018;215:90–101. https://doi.org/10.1016/j.fuel.2017.11.023.

[14] Al Qubeissi M, Sazhin SS, Al-Esawi N, Kolodnytska R, Khanal B, Ghaleeh M, et al. Heating and Evaporation of Droplets of Multicomponent and Blended Fuels: A Review of Recent Modeling Approaches. Energy & Fuels 2021;35:18220–56. https://doi.org/10.1021/acs.energyfuels.1c02316.

[15] Sallevelt JLHP, Gudde JEP, Pozarlik AK, Brem G. The impact of spray quality on the combustion of a viscous biofuel in a micro gas turbine. Appl Energy 2014;132:575–85. https://doi.org/https://doi.org/10.1016/j.apenergy.2014.07.030.

[16] Daho T, Vaitilingom G, Sanogo O, Ouiminga SK, Segda BG, Valette J, et al. Study of droplet vaporization of various vegetable oils and blends of domestic fuel oil–cottonseed oil under different ambient temperature conditions. Biomass Bioenergy 2012;46:653–63. https://doi.org/10.1016/J.BIOMBIOE.2012.06.031.

[17] Manjunath M, Raghavan V, Mehta PS. Vaporization characteristics of suspended droplets of biodiesel fuels of Indian origin and their diesel blends – An experimental study. Int J Heat Mass Transf 2015;88:28–41. https://doi.org/10.1016/J.IJHEATMASSTRANSFER.2015.04.052.

[18] Wang X, Wang G, Wang L, Zhang J, Yan J. Ethanol Evaporation Characteristics of the Blends of Fatty Acid Methyl Ester and Ethanol. J Shanghai Jiaotong Univ Sci 2021;26:210–7. https://doi.org/10.1007/s12204-021-2281-9.

[19] Nomura H, Ujiie Y, Rath HJ, Sato J, Kono M. Experimental study on high-pressure droplet evaporation using microgravity conditions. Symposium (International) on Combustion 1996;26:1267–73. https://doi.org/10.1016/S0082-0784(96)80344-4.

[20] Verwey C, Birouk M. Fuel vaporization: Effect of droplet size and turbulence at elevated temperature and pressure. Combust Flame 2018;189:33–45. https://doi.org/10.1016/j.combustflame.2017.10.010.

[21] Yu D, Chen Z. Theoretical analysis on droplet vaporization at elevated temperatures and pressures. Int J Heat Mass Transf 2021;164:120542. https://doi.org/10.1016/j.ijheatmasstransfer.2020.120542.

[22] Luning Prak DJ, Cowart JS, Hamilton LJ, Hoang DT, Brown EK, Trulove PC. Development of a Surrogate Mixture for Algal-Based Hydrotreated Renewable Diesel. Energy & Fuels 2013;27:954–61. https://doi.org/10.1021/ef301879g.

[23] Abdul Jameel AG, Elbaz AM, Emwas A-H, Roberts WL, Sarathy SM. Calculation of Average Molecular Parameters, Functional Groups, and a Surrogate Molecule for Heavy Fuel Oils Using 1H and 13C Nuclear Magnetic Resonance Spectroscopy. Energy & Fuels 2016;30:3894–905. https://doi.org/10.1021/acs.energyfuels.6b00303.

[24] El-Banbi A, Alzahabi A, El-Maraghi A. Dry Gases. In: Katie Hammon, editor. PVT Property Correlations, Elsevier; 2018, p. 29–63. https://doi.org/10.1016/B978-0-12-812572-4.00003-5.

[25] Riazi MR, Daubert TE. Characterization parameters for petroleum fractions. Ind Eng Chem Res 1987;26:755–9. https://doi.org/10.1021/ie00064a023.

[26] Yu J, Eser S. Determination of Critical Properties (Tc, Pc) of Some Jet Fuels. Ind Eng Chem Res 1995;34:404–9. https://doi.org/10.1021/ie00040a045.

[27] Hashimoto N, Nomura H, Suzuki M, Matsumoto T, Nishida H, Ozawa Y. Evaporation characteristics of a palm methyl ester droplet at high ambient temperatures. Fuel 2015;143:202–10. https://doi.org/10.1016/j.fuel.2014.11.057.

[28] Ambrose D, Townsend R. Critical temperatures and pressures of some alkanes. Transactions of the Faraday Society 1968;64:2622–31. https://doi.org/10.1039/TF9686402622.

[29] Poling BE, Prausnitz JM, O'Connell JP. Properties of Gases and Liquids. 5th Edition. New York: McGraw-Hill Education; 2001.

[30] Yaws CL, editor. Chemical Properties Handbook. 1st Edition. New York: McGraw-Hill Education; 1999.

[31] Mrzljak Vedran, Ţarković Boţica, Prpić-Oršić Jasna. LIQUID FUEL TEMPERATURE, PRESSURE AND INJECTION RATE INFLUENCE ON INJECTOR NOZZLE REYNOLDS NUMBER AND CONTRACTION COEFFICIENT. International Scientific Journals of Scientific Technical Union of Mechanical Engineering "Industry 40" 2018;3:138–41.

[32] Naito Y, Ueda K, Hashimoto N, Takagi M, Kawauchi S, Imai Y, et al. Experimental Study on Evaporation Characteristics of Light Cycle Oil Droplet under Various Ambient Conditions. Energy & Fuels 2021;35:6219–30. https://doi.org/10.1021/acs.energyfuels.0c04406.

[33] MORIN∗ C, CHAUVEAU C, DAGAUT P, GÖKALP I, CATHONNET M. VAPORIZATION AND OXIDATION OF LIQUID FUEL DROPLETS AT HIGH TEMPERATURE AND HIGH PRESSURE: APPLICATION TO *N* -ALKANES AND VEGETABLE OIL METHYL ESTERS. Combustion Science

and Technology 2004;176:499–529. https://doi.org/10.1080/00102200490276719.

[34] GHASSEMI H, BAEK SW, KHAN QS. EXPERIMENTAL STUDY ON BINARY DROPLET EVAPORATION AT ELEVATED PRESSURES AND TEMPERATURES. Combustion Science and Technology 2006;178:1031–53. https://doi.org/10.1080/00102200500296697.

[35] Long W, Yi P, Jia M, Feng L, Cui J. An enhanced multi-component vaporization model for high temperature and pressure conditions. Int J Heat Mass Transf 2015;90:857–71. https://doi.org/10.1016/j.ijheatmasstransfer.2015.07.038.

[36] Zhang Y, Chen F, Jia M, He Z, Yi P. Molecular dynamics investigation of the vaporization characteristics of *n* -alkane blended fuels under different ambient conditions. AIP Adv 2022;12:075309. https://doi.org/10.1063/5.0098054.

[37] Pinheiro AP, Vedovoto JM, da Silveira Neto A, van Wachem BGM. Ethanol droplet evaporation: Effects of ambient temperature, pressure and fuel vapor concentration. Int J Heat Mass Transf 2019;143:118472. https://doi.org/10.1016/j.ijheatmasstransfer.2019.118472.

[38] Kitano T, Nishio J, Kurose R, Komori S. Effects of ambient pressure, gas temperature and combustion reaction on droplet evaporation. Combust Flame 2014;161:551–64. https://doi.org/10.1016/j.combustflame.2013.09.009.

[39] Yi P, Jia M, Long W, Qiao L, Yang T, Feng L. Evaporation of pure and blended droplets of diesel and alcohols (C2–C9) under diesel engine conditions. Numeri Heat Transf A Appl 2017;71:311–26. https://doi.org/10.1080/10407782.2016.1264749.

[40] He X, Feng H, Liu Z, Wang H, Li X, Zeng F, et al. Numerical simulation of the evaporation characteristics of a dimethyl ether droplet in supercritical environment. Fuel 2020;267:117120. https://doi.org/10.1016/j.fuel.2020.117120.